Construction of a linear plasma device for studying helicon plasmas relevant to plasma wakefield accelerators

Jonathan Green and Oliver Schmitz

Engineering Physics Department, University of Wisconsin - Madison.

Abstract. The Magnetized AnisotRopic Ion Apparatus (MARIA) was constructed to study the density buildup and particle balance in helicon plasmas. This device will help address key questions surrounding the dynamics of the neutral argon population and the role it plays in defining the ultimate density achieved. Insights gained from this research are particularly important for meeting the demanding high density and high uniformity requirements of plasma based wakefield accelerator concepts. A key feature of the MARIA device is it's fully transparent borosilicate glass chamber which enables the flexible use and development of optical techniques for measuring plasma parameters like electron temperature and density. Wistler-mode behavior featuring very high on-axis ionization fraction and a linear relationship between electron density and magnetic field strength up to 5×10^{18} m^{-3} has been demonstrated through the use of an RF compensated Langmuir probe. Laser induced fluorescence measurements, which build on the Langmuir probe measurements, are able to fully constrain the 2D particle balance by enabling ion and neutral sources and sinks to be spatially resolved. Initial flux measurements in the axial direction are presented, while efforts to increase the resolution of radial flux measurements is ongoing. Near term structural enhancements include a water cooled antenna which will enable CW operation up to 10 kW.

Submitted to: *Plasma Sources Sci. Technol.*

1. Introduction

High density plasma sources that can operate efficiently at constant power are essential for advancing a variety of plasma science and technology research objectives. In particular, the development of longitudinally uniform high density sources, i.e. along the chamber axis, is urgently needed to realize the benefits of plasma wakefield accelerators [1]. To achieve electron energies of hundreds of gigaelectron volts (GeV), new plasma sources that can maintain uniform electron densities in the mid 10^{20} m^{-3} range, with an axial electron density variation of $\Delta n_e \leq 0.25\%$, over tens or hundreds of meters must be developed [2]. Few existing plasma technologies have the necessary characteristics to scale to these lengths. Buttenschön *et al* have demonstrated the ability of pulsed helicon plasmas to achieve the necessary density of 7×10^{20} m^{-3} [3]. However, little research has been focused on improving the poor longitudinal uniformity seen in experiment [4, 5]. The Magnetized AnisotRopic Ion Apparatus (MARIA) device has recently been overhauled and upgraded to help identify the underlying physics leading to the poor uniformity and develop techniques to improve it.

A major research topic for MARIA is the role neutral atom fueling and depletion plays in establishing the ultimate electron density profile. Several authors have indentified the phenomenon of neutral depletion often experienced in helicon plasmas [6, 7, 8]. Dr. Scime's group at West Virginia University has done extensive experimental work identifying the onset and etxtent of neutral depletion in helicon plasmas [9, 10, 11]. Chen *et al* have hypothesized an explanation based on ionization alone [12], while Magee *et al* have suggested neutral expulsion, e.g. from collisions, also plays a role [10]. To properly investigate this topic a primary requirement for MARIA is the ability to scale from a neutral dominated, low ion fraction, plasma to an ion dominated, high ion fraction, plasma. A secondary requirement is achieving electron densities in the 10^{19} m^{-3} range to operate as close to accelerator relevant plasma conditions as possible without excessive investment in plasma heating infrastructure.

Operation of MARIA is not solely dedicated to wakefield accelerator research. Other research topics performed on this device include aiding validation and development of atomic models used for line ratio plasma diagnostics [13], plasma material interaction studies, and basic plasma physics investigation. As such, MARIA must be flexible in terms of the operating gas, pre-fill pressure, vacuum pumping arrangement, and diagnostic access.

2. Background

Helicon plasmas are heated by propagating a whistler wave in a uniform magnetic field [12, 14, 15, 16]. The resulting plasma typically has high electron density, in the range of $10^{17}-10^{20}$ m^{-3}, and electron temperatures between 1-10 eV. The wave structure follows that of the right-hand circularly polarized R-wave for which the dispersion relation is

$$\frac{c^2k^2}{\omega^2} = 1 - \frac{\omega_p^2/\omega^2}{1-\omega_c/\omega\cos\theta}, \tag{1}$$

where c is the speed of light in vacuum, k is the wave number, ω is the frequency, ω_p is the electron plasma frequency, ω_c is the electron cyclotron frequency, and θ is the angle between $\mathbf{k}$ and $\mathbf{B}$.

The simplified version of significant experimental and theoretical work done in the 1960-1970s [17, 15, 18, 19] is that if the wave frequency is far below the electron cyclotron frequency, and the effect of electron inertia is neglected, the dispersion relation can be reduced to

$$k = \frac{\omega_p^2\omega}{c^2\omega_c k_\parallel} = \frac{\omega}{k_\parallel}\frac{n_e e\mu_0}{B}, \tag{2}$$

where $k_\parallel = k\cos(\theta)$ is the parallel wavenumber, θ is the angle between $\mathbf{k}$ and $\mathbf{B}$, n_e is the electron density, B is the applied magnetic field strength, and e and μ_0 are the electron charge and the vacuum permeability respectively. For fixed excitation frequency and assuming $k_\parallel$ is related to the antenna length, this yields the familiar n_e/B scaling for helicon plasmas.

It was later shown that carrying the electron inertia through the calculations gives rise to the so-called Trivelpiece-Gould (TG) mode [20, 12]. Blackwell *et al* later detected the TG mode experimentally at low magnetic field strength [21], but concluded that the helicon wave, with the dispersion relation given by Equation 2, dominates near the axis at higher magnetic field strengths.

The RF power coupling contributed by the helicon and TG modes and the details of the coupling mechanism itself is still an evolving subject [22, 23]. However, due to the relatively high magnetic field strengths used in this work, $B \geq 400$ G, the helicon mode is assumed to dominate.

3. Apparatus

The locations of major features of the MARIA chamber are shown in a partial cross section in Figure 1.

The main vacuum chamber is constructed from four 14 cm diameter sections of borosilicate glass. A single borosilicate glass 'cross' section is connected to one end of the main chamber via a 14 cm stainless steel bellows section and contains all the vacuum

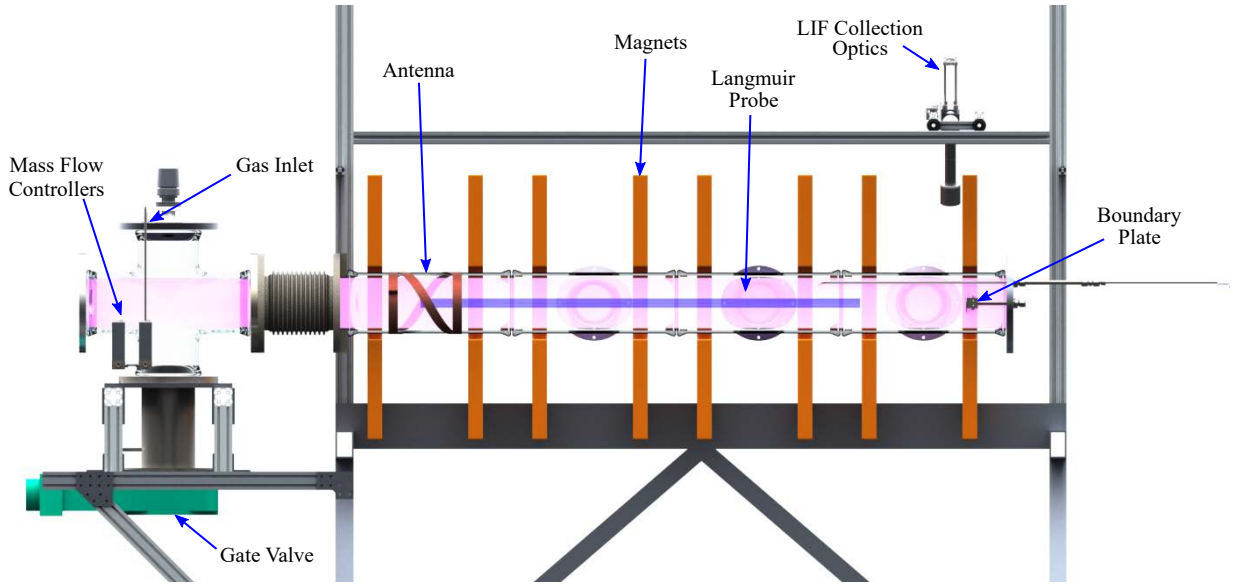

Figure 1: A partial cross section of the MARIA plasma device. The magnetic field is oriented left to right inside the chamber in this view and defined the 'downstream' direction. The vacuum turbo pump is mounted below the green gate valve labelled on the left of the figure.

infrastructure. The vacuum pump, shown at the bottom of cross cross on the end of the device, is a 140 l/s Alcatel 5150CP turbomolecular pump. The turbo-pump is backed by a 1 l/s roughing pump. The primary pressure gauge is an Agilent FRG 702 inverted magnetron/pirani gauge mounted to the top of the pumping cross. The base pressure is typically around 5×10^{-7} Torr.

Gas is metered into the chamber by an MKS GE50A thermal mass flow controller mounted at the same end and above the vacuum pumps, as indicated in Figure 1. Multiple flow controllers are connected to a manifold with a single stainless steel tube making the final connection to the chamber at the top of the pumping cross. The gas manifold allows the operating gas to be changed quickly and enables precisely metered gas mixtures to be used. Current gasses include argon, hydrogen, and helium. To ensure the device can be safely operated with hydrogen, a fully grounded gas delivery system with crush-resistant tubing and a dedicated exhaust gas removal system was constructed according to best practices. Typical gas flow rates of $\sim$ 40 sccm yield operating pressures of $\sim$ 2.0 mTorr.

Locating the gas source and vacuum pump at the same end of the MARIA experiment establishes a uniform neutral pressure in the main chamber. By eliminating neutral pressure gradients due to the vacuum operation, flows and density gradients measured during plasma operation are the result of the plasma itself.

Surrounding the main chamber are eight pancake electromagnets able to generate a peak magnetic field of 1005 G, limited only by the existing power supplies. The on-axis magnetic field strength at the maximum current presently available is shown in Figure 2. Due to the chamber geometry, the magnets cannot be placed to produce a uniform field. Between the first two magnets and last two magnets the field strength on axis reduces to 625 Gauss at 18 and 158 cm respectively. The magnets are arranged in four parallel sets of two magnets in series. At 950 A of total current, each coil is carrying 238 A of current.

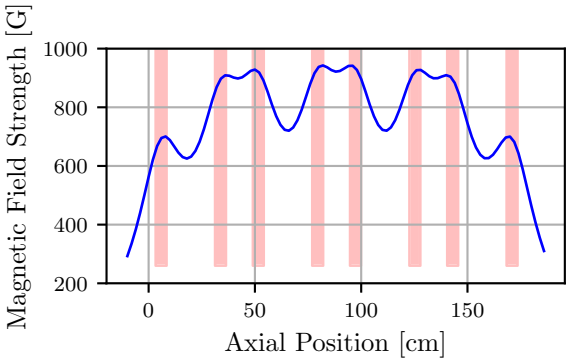

Figure 2: The on-axis magnetic field strength at 938 amps of total current (235 A per coil). Due to geometric constraints, the magnets, indicated by the shaded red bars, cannot be placed to create a uniform magnetic field.

As with any RF system, inattention to the

grounding scheme can give rise to ground loops which cause serious interference with diagnostics and can potentially be hazardous to equipment operators. The electrical configuration for MARIA, shown in Figure 3, follows a single point star type grounding topology. A grounded mesh screen surrounding the plasma chamber, which serves as a Faraday shield to contain RF radiation, was chosen as the single point ground 'plane' from which all ground references are derived. The one exception to this rule is that the RF generator is separately grounded through it's electrical power connection to adhere to the local electrical code. A ferrite ring is installed around the coax cable connecting the RF generator to the matching network to guard against any common mode RF currents that might arise due to this ground loop.

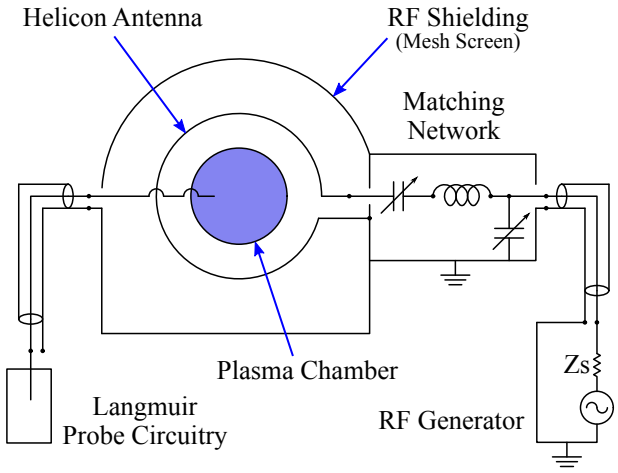

Figure 3: A simplified schematic of MARIA's electrical system. The RF shielding forms the RF 'ground plane' from which all other components source their ground reference. The L-type matching network is directly connected to the helicon antenna.

The antenna is a helical antenna designed to couple to the $m = +1$ helicon mode. The antenna is 18 cm long and 14 cm in diameter and constructed of 1.5 mm thick copper strap that is soldered together. The antenna is cooled by forced convection, which limits the CW power to ~ 2 kW. RF power beyond 2 kW can be coupled to the plasma for shorter durations. While the RF generator output has a 50 ohm impedance, the antenna alone has a very different impedance and the coupling to the plasma has a further impact. To enable impedance matching between the RF generator and the antenna/plasma system, a tunable L-type matching network was employed. 15 kV variable vacuum capacitors were arranged as shown in Figure 3, while the fixed inductor is simply the ~ 45 nH self inductance of the flat metal plate the two capacitors are mounted to.

4. Diagnostics

The diagnostics on MARIA are predominantly spectroscopic with the exception of a single tip RF compensated Langmuir probe. As discussed above, one of the principle objectives is to investigate the spatial distribution of particle fluxes and constrain the particle balance. To do this, flexible, spatially resolved, diagnostics are important and spectroscopic techniques are well suited for this task.

4.1. RF Compensated Langmuir Probe

The baseline diagnostic on MARIA is a single tip RF compensated Langmuir probe. The design, shown as a CAD rendering in Figure 4, is based on the RF compensated Langmuir probe work of Chen *et al* [24, 25, 26]. The probe body is a 6.35 mm stainless steel tube surrounded by a quartz tube to electrically insulate it from the plasma. An alumina tube, through which the probe tip passes, is inserted into the end of the stainless steel tube and held in place with Torr-Seal. The tip is 3 mm long, 0.5 mm in diameter, and made of tungsten. The RF compensation electrode is a 6 mm wide by .1 mm tantalum foil wrapped around the alumina tube near the probe tip.

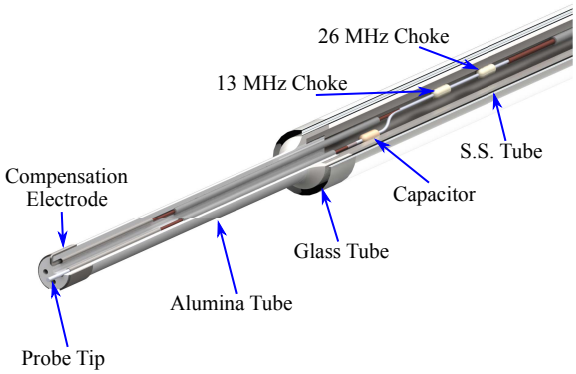

Figure 4: The construction of the RF Compensated Langmuir Probe is shown here in a partial section view. Electrical components residing in the stainless steel tube were insulated with heat-shrink tubing.

The probe electrical design, shown in Figure 5,

is centered around two differential amplifiers. One differential amplifier measures the probe current by measuring the voltage drop across a 15 ohm resistor. The other amplifier measures the DC probe bias voltage by measuring the voltage drop across a 1 mega-ohm resister which is part of a 10:1 voltage divider. The output of the differential amplifiers are connected to the data acquisition system via coaxial cables. The probe bias is provided by a Kepco BOP100M ±100 V bipolar power supply. RF chokes were installed within 6 inches of the probe tip with resonant frequencies of 13.2 MHz and 26 MHz. Ideally these chokes would have resonant frequencies of exactly 13.56 MHz and 27 MHz to block oscillations from the RF system, but the need to locate the chokes near the probe tips forced the use of commercially available chokes with a limited selection of resonant frequencies. A 1 nF capacitor couples the compensation electrode to the probe tips before the RF chokes.

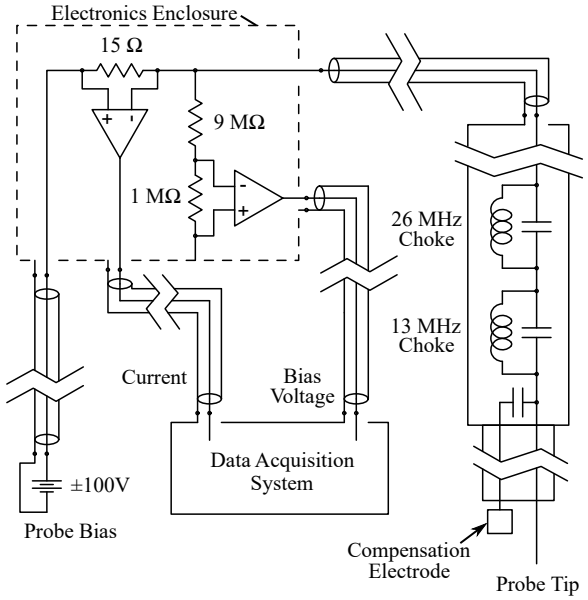

Figure 5: The RF compensated Langmuir probe electrical schematic.

The principle concern is that the plasma potential will oscillate due to the RF heating source. As a Langmuir probe bias voltage is swept, the current collected by the probe is significantly distorted from the ideal exponential electron collection current due to the oscillating plasma potential. Analysis using the distorted current-voltage (I-V) can then lead to erroneously high electron temperature measurements. This effect is well described in a book section written by Professor Noah Hershkowitz at the University of Wisconsin - Madison [27]. By installing the RF chokes, the probe tip is effectively decoupled from the sensing electronics at the choke's resonant frequencies and allowed to float. By including a large compensation electrode, and coupling it to the probe tip by a small capacitor, sufficient electrons are collected to drive the probe tip to follow the plasma potential.

4.2. Laser Induced Fluorescence

The workhorse diagnostic for measuring particle flux is laser induced fluorescence (LIF). LIF techniques have been used to study the properties of atoms and molecules since at least 1968 [28]. On MARIA, a master oscillator power amplifier (MOPA) arrangement using a narrow bandwidth diode laser and a tapered chip amplifier formed the laser light source. This arrangement was highlighted by Severn *et al* for it's ability to measure high quality velocity distribution functions (VDFs) at low cost compared to dye laser sources [29], The seed laser is a Toptica DL100 diode laser operating in a single mode and having a line width on the order of 100 kHz. The amplifier is a Toptica BoosTA tapered chip amplifier which maintains spectral purity of the seed laser while boosting the output power to $\sim$ 400 mW. Tuning this laser system to 667.912 nm and 668.614 nm enables VDFs to be acquired for neutral and singly ionized argon atoms respectively. Further details of the LIF system and the analysis technique are described in a paper by Green *et al* [30].

4.3. Emission Spectroscopy

In addition to active spectroscopy via LIF, multiple Czerny-Turner type spectrometers are available for use on MARIA. The primary spectrometer is a .5 m Acton SP2500i from Princeton Instruments with an integral turret containing three gratings and can be fitted with one of two interchangeable CCD detectors. The first CCD is a PIXIS 256E which can be cooled to -70° C and is sensitive to photons between 250 nm and 1000 nm. The second CCD is a PI-MAX2 intensified CCD which can be gated down to 2 ns exposures and is sensitive to photons between 300 nm and 700 nm. The three gratings currently installed are a 1800 groove/mm holographic grating blazed at 500 nm, a 1200 groove/mm grating blazed at 500 nm, and a 1200 groove/mm grating blazed at 300 nm. Two secondary compact USB spectrometers are also available and cover the ranges of 350 nm to 750 nm and 500 nm to 1000 nm. These spectrometers lower resolution but are useful for acquiring broad survey spectra of the plasma.

The .5 m spectrometer is fiber coupled to the plasma with up to 15 independent channels. At present, only five of these channels are used to take simultaneous spectra at different axial positions on

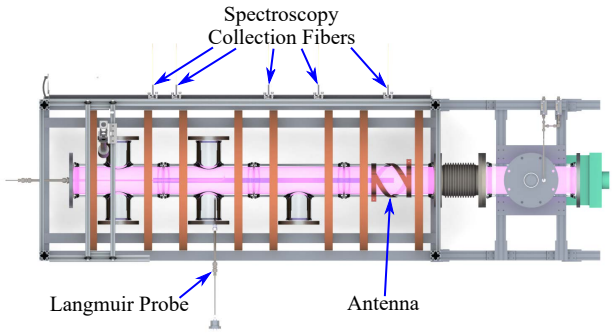

Figure 6: Five of the 15 available spectroscopy channels are currently arranged along the axis of MARIA to record line integrated spectra. The optics are all carefully aligned and can be tilted ±15 degrees to record data appropriate for Abel transformation.

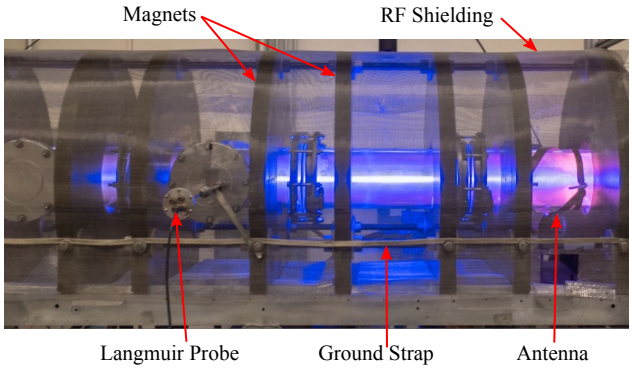

Figure 7: Typical appearance of MARIA plasmas at 700 W of RF power, 700 G magnetic field strength, and 2.0 mTorr neutral pressure. The bright blue core is due to singly ionized argon emission on the axis of the device. The antenna is located on the right and the downstream boundary plate is on the left in this view.

MARIA. The position of the five channels in use are shown in Figure 6. The collimating lenses are mounted to a piece of 80/20 material and their axial positions can be changed easily. Additionally the 80/20 material itself can be rotated ±15 degrees to record spectra from different chords. Multiple such spectra can then be inverted via an Abel transformation to infer the radial distribution of plasma parameters. Emission spectra from the plasma are typically analyzed using line ratio spectroscopy to infer electron density and temperature. Additionally the high resolution of the .5 m spectrometer allows for the unambiguous identification of emission lines from sputtered impurity atoms.

5. Initial Results

The plasmas generated by MARIA are visually quite striking, as seen in Figure 7. The plasma shown in the photograph is heated by 700 W of RF power, has a magnetic field strength of 700 G, and 2.0 mTorr of argon. A distinct blue core that extends nearly the full length of the device is visible. The intensity of the blue Ar II emission is brightest just downstream of the antenna (to the left in this picture) and tends to fade out with increasing distance from the antenna. The pinkish emission from neutral argon is visible at the far left and right in the photograph.

The Langmuir probe, magnets, RF shielding and antenna are also indicated in Figure 7. As explained above, the RF shielding works to contain the RF radiation and minimize electromagnetic interference with other devices. This shielding was found to be quite important as the optical mouse used on the control computer is particularly susceptible to RF interference, and can temporarily stop relaying user inputs. The ground strap indicated in Figure 7 helps secure the shielding in place and electrically grounds components that do not directly contact the shielding.

With the recent completion of a computer controlled chilled water cooling system with a capacity of 50 kW, argon plasmas have been reliably sustained for over 7 hours. These long duration plasmas have been heated by 700 W of RF power at 700 G and the plasma was only terminated because data gathering had been completed. Plasmas with higher heating power are limited by the heat dissipated by the antenna and the inadequate cooling provided by forced convection. Water cooling for the antenna is currently being implemented and once completed will allow for CW operation up to 10 kW. Argon is the typical operating gas, however plasma operation with helium and hydrogen has been successfully tested.

Electron density and temperature measurements made with the Langmuir probe from an initial parameter scan is shown in Figures 8A and 8B respectively. For this scan, the RF heating power was varied between 300 W and 900 W while the magnetic field strength was varied between 300 G and 800 G. For heating power below 1 kW, typical electron temperatures are below 5 eV. As a result of the helicon wave propagation dependence on the applied magnetic field, electron densities between 10^{17} and 5×10^{18} m^{-3} are accessible by varying the magnetic field strength. While the electron temperature is relatively independent of RF heating power and magnetic field strength, the electron density is approximately linearly dependent on both parameters beyond a certain threshold. An inverse relationship exists between the RF heating power and the magnetic field strength

necessary to achieve a given electron density. For low RF heating power, around 300 W, a magnetic field strength of 800 G is necessary to yield an electron density of 10^{18} m^{-3}. Increasing the RF heating power to 700 W reduces the required magnetic field strength to achieve an electron density of 10^{18} m^{-3} to 450 G.

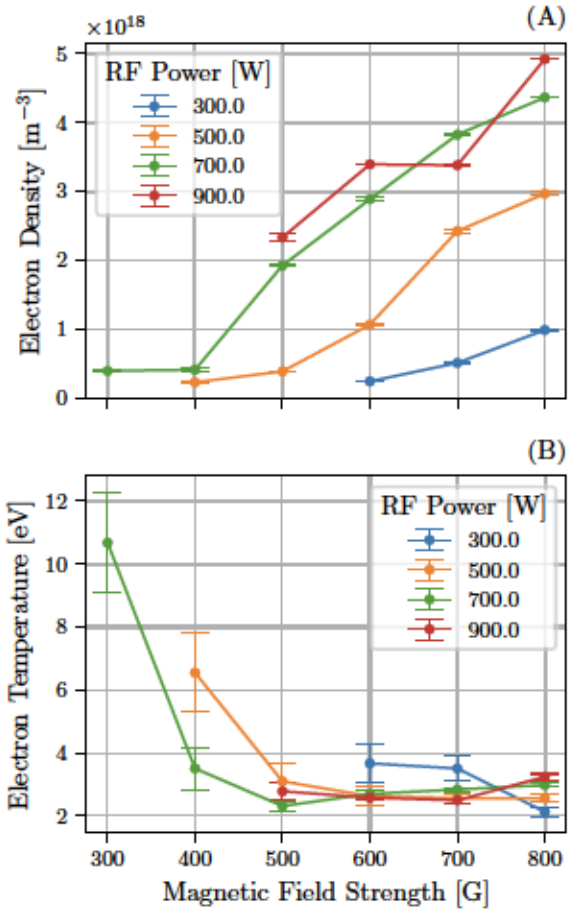

Figure 8: The typical operational domain of the MARIA device with an air cooled antenna. The jump into helicon mode is evident by the factor of 10 jump in electron density between 400 G and 500 G at 700 W.

The radial electron density and temperature profiles are shown in Figure 9A and 9B respectively. MARIA plasmas exhibit axially peaked electron densities, n_e, at all magnetic field strengths, however the radial gradient is much steeper above 450 G when the helicon mode is propagating. The radial electron temperature, T_e, exhibits more structure with a maximum close to the chamber wall, a minimum at approximately 1/2 the chamber radius, and a local maximum on axis. The distinct electron density jump between 450 G and 500 G is characteristic of the abrupt jump into the helicon mode of operation. The abrupt increase in density followed by a linear relationship between density and magnetic field strength, $n_e \propto |B|$ is currently the best indication of helicon operation on MARIA. The density jump also coincides with an abrupt visual change in plasma structure from a diffuse pinkish plasma, dominated by neutral argon emission, to having an intensely blue core, dominated by singly ionized argon emission, as seen in Figure 7. This visual indication is often the more immediate and easier way to identify the onset of helicon operation. Establishing a $\dot{B}$ to confirm the helicon mode by sensing the wave fields directly is currently underway.

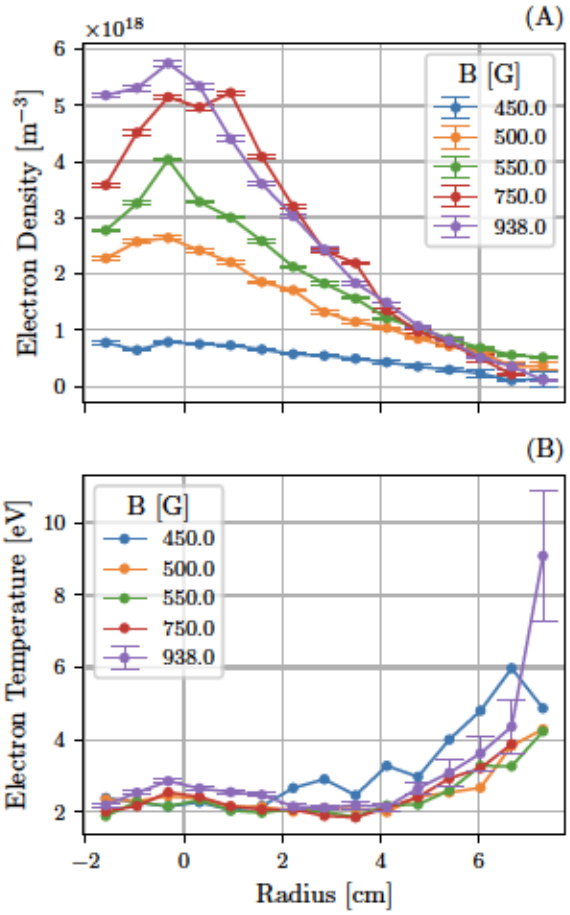

Figure 9: Radial variation of electron temperature, A.), and density, B.), at several magnetic field strengths. RF power was held at 700 W and the neutral pressure was held at 2.0 mTorr.

While the Langmuir probe can provide general information on the electron density and temperature, passive specroscopy provides a broader understanding of the atomic populations present in the plasma. Figure 10A shows the radial emission profile of the 811.8 nm $4s^2[3/2]\,2$ to $4p^2[5/2]\,3$ neutral argon transition at several axial locations. The 225.0 mm

trace is located in the middle of the antenna and has some additional radial structure between 3-6 cm. The cause of the extra bump in the curve is not currently known but indicates a change in the atomic processes leading to emission of 811.8 nm photons. This could be a result of local differences in electron temperature. Figure 10B shows the radial emission profile for the 488.1 nm $4p^2[D]\,5/2$ to $4s^2[P]\,3/2$ singly ionized argon transition. By comparing Figure 10B and 9A it is clear that the Ar II emission does not follow the electron density profile measured by the Langmuir probe, with the emission intensity being much more concentrated near the axis. However, since the ion emission is proportional to the density of ions and electrons, $I \propto n_e n_i$, comparing the electron density with the square root of the ion emission intensity is a better match. The Langmuir probe is located at 1012 mm, so is approximately midway between the highly peaked 830 mm trace and the flatter 1297 mm trace.

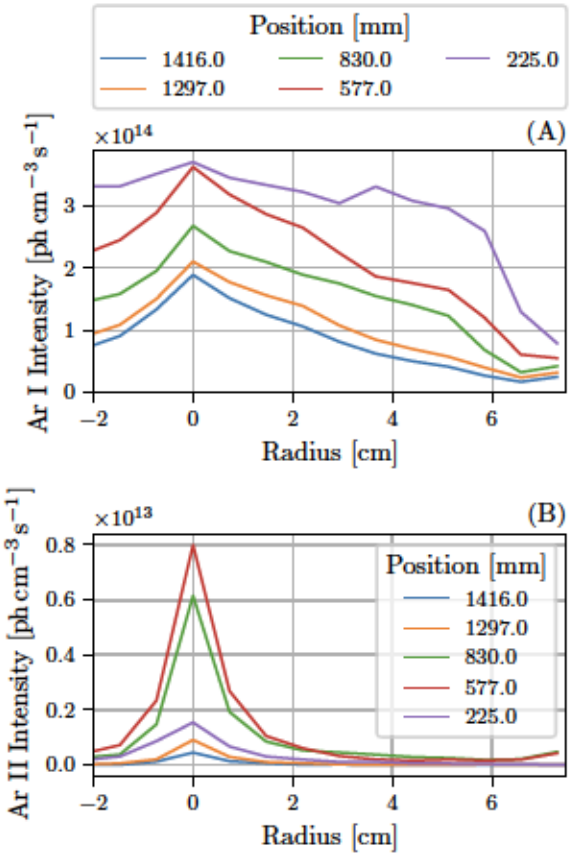

Figure 10: A.) Radial emission profile of the 811.8 neutral argon line. B.) Radial emission profile of the 488.1 singly ionized argon line. This data was taken during the course of a CW plasma discharge.

LIF intensity and flux measurements taken at several axial locations with a constant 700 W of RF heating power and several magnetic field strengths are shown in Figures 11a and 11B respectively. At magnetic field strengths around 450 G and below, the density of $3d^4[F]\,7/2$ ions available to by pumped by the laser is very low and the LIF intensity is equally weak all along the axis. Below this threshold magnetic field strength and with 700 W of RF heating power, the signal to noise ratio is insufficient for curve fitting and data analysis. Above the 450 G threshold, both the LIF intensity and flux increased strongly with increasing magnetic field strength. The maximum LIF intensity is achieved near 650 mm at 450 G and shifts further downstream to 1050 mm at 938 G. This shift in the axial location of peak intensity corresponds to a significant increase in the flux of ions moving parallel to the magnetic field. At axial positions beyond 1400 mm, the rapid increase of parallel ion flux is likely due pre-sheath and pressure gradient effects. The flux of ions leaving the plasma increases by a factor of two for the same factor increase in magnetic field and is predominantly due to the increase in density, not an increase in flow velocity.

The zero crossing near 900 mm and the clear gradient in Figure 11B can be explained through the mass conservation equation. By neglecting the temporal component, $\frac{\partial n}{\partial t}$, since the plasma is operated in CW and the measurement is on the order of minutes, the mass conservation equation is simply

$$\frac{\partial}{\partial z}(nV_z) + \frac{1}{r}\frac{\partial}{\partial r}(rnV_r) = S(r,z). \tag{3}$$

Here, V_z and V_r are the axial and radial flow velocities respectively, r is the radial position, n is the ion density, and $S(r,z)$ is the ion source rate. Since the left hand of the equation has terms that are separately functions of axial and radial flux, the axial flux gradient seen in Figure 11B is already an indication of an ionization source in this region. However, accurate radial flux data is necessary to accurately measure the ionization source rate and is the topic of an upcoming paper.

Retuning the LIF laser to 667.912 nm enables the $4s^2[3/2]\,1$ to $4p^2[1/2]\,0$ neutral argon transition to be pumped. The LIF intensity is shown in Figure 12A. At low magnetic field strengths around 450 G, sufficient neutral atoms in the $4s^2[3/2]\,1$ level are present between 680 mm and the plate at 1680 mm to yield a measureable LIF signal. As the magnetic field strength increases, the LIF signal strength peaks around 550 G and is concentrated near an axial position of 1560 mm. Beyond 550 G the LIF intensity rapidly decreases and further concentrates near the target plate.

As a consequence of flow velocities below 150

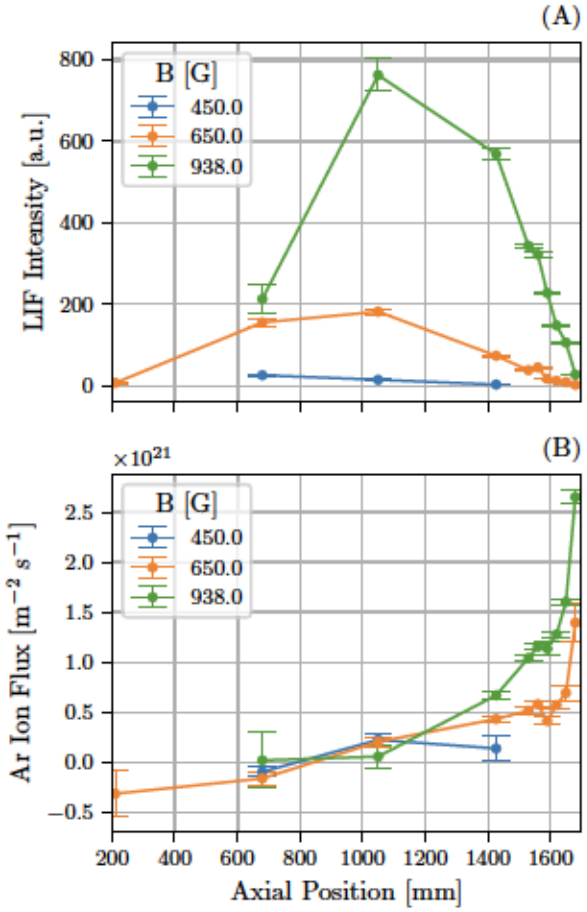

Figure 11: LIF fluorescence intensity, A.), and flow velocity, B.), of the $3d\,^4F\ 7/2$ to $4p\,^4D\,5/2$ singly ionized argon absorption transition for several magnetic field strengths. RF power was held at 700 W and neutral pressure was held at 2.0 mTorr.

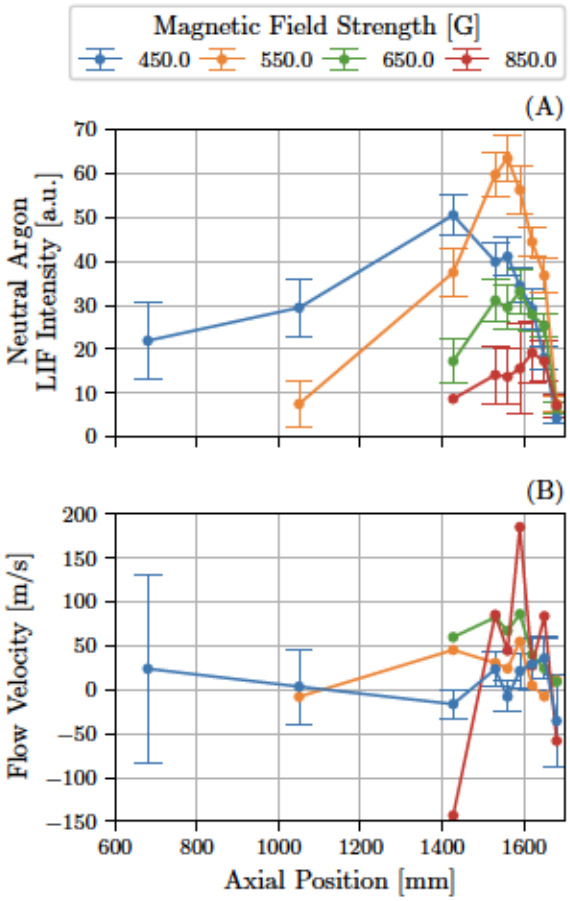

Figure 12: Fluorescence intensity, A.), and flow velocity, B.) for the $4s\,^2[3/2]\,1$ to $4p\,^2[1/2]\,0$ neutral argon absorption transition. RF heating power was 700 W and neutral fill pressure was 2.0 mTorr. Typical flow velocity error bars are show shown on the 450 G trace.

m/s, the LIF based flow velocity measurement is very sensitive to random fluctuations in the LIF signal leading to the scatter in the data shown in Figure 12B. A distinctly positive flow velocity, towards the boundary plate, is measured between 1500 and 1650 mm. At 1680 mm, immediately in front of the target plate located at 1684 mm, a negative flow velocity is measured at all magnetic field strengths. This suggests a flow reversal is occurring in this region, however signal to noise ratio improvements and additional measurements are needed to further investigate the apparent reversal.

The intense flux of argon ions into the downstream target plate can result sputtering of even robust materials like molybdenum. The target plate was initially constructed of AISI-316L stainless steel, which contains up to 18% chromium by weight. During plasma operation a distinct green glow appeared next to the target plate, shown in Figure 13A. Spectroscopic measurements confirmed the greenish tinge to be from neutral chromium emission at 520.6, 520.7, and 521 nm. After switching from stainless steel to molybdenum sputtering of molybdenum was identified by the three characteristic neutral molybdenum lines at 550.8, 553.4, and 557.2 nm.

The sputtering observed on MARIA is linked to the imposed electrical potential of the target plate. Sputtering is only observed when the target plate is held at ground potential. Sputtered material is then deposited nearby on the glass chamber walls, obscuring the view of the LIF system. Sputtering is not observed when the target plate is floated by mounting it to the chamber using an insulating polyether ether ketone (PEEK) material. The floated configuration is desireable for LIF studies but this

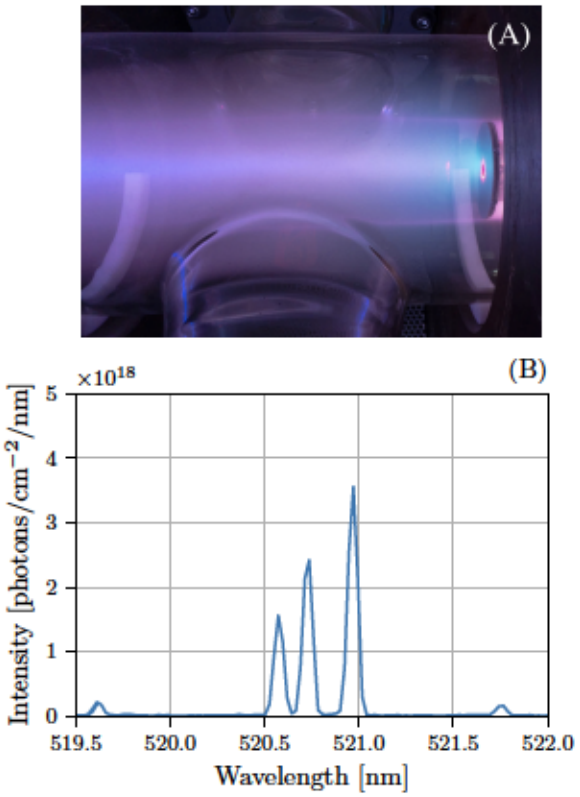

Figure 13: A.) With the boundary plate grounded, preferential sputtering of chromium from AISI 316L stainless steel is apparent from the greenish glow near the boundary plate. B.) The presence of the three prominent chromium emission lines near 520 nm confirms the type of metal being sputtered.

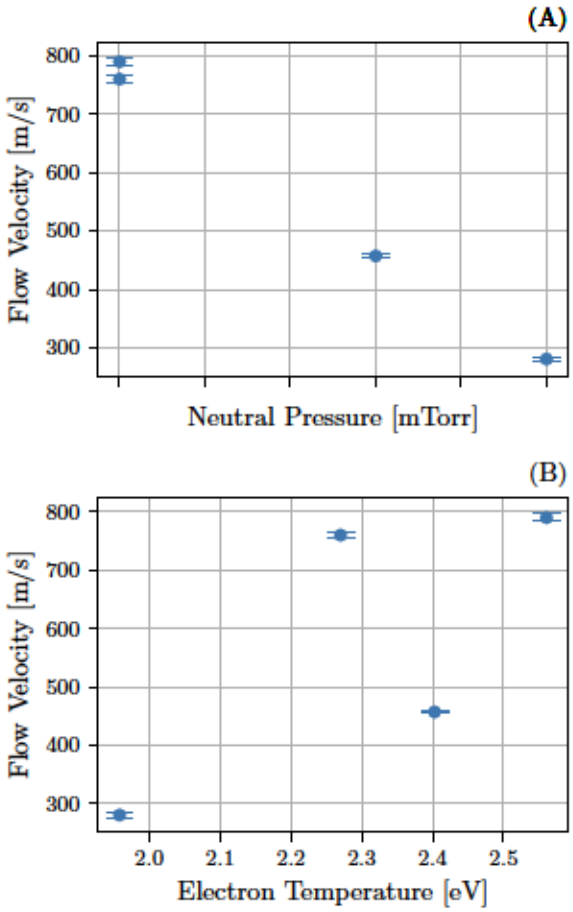

Figure 14: A.) Linear dependence of argon ion flow velocity on neutral gas fill pressure. B.) The change in flow velocity did not appear to match the $(T_e)^{1/2}$ scaling of the ion sound speed.

sputtering effect represents an attractive opportunity to perform plasma-material interaction studies.

The effect of pressure and electron temperature on the ion flow velocity was briefly considered while investigating how to minimize the target sputtering. LIF flow velocity measurements, shown in Figure 14A, indicate an inverse relationship between flow velocity and neutral fill pressure. The flow velocity measurements were all taken at the same location, an axial position of 1630 mm, the same RF power, 700 W, and the same magnetic field strength, 700 G. It is reasonable to wonder whether a change in electron temperature has some effect, via the ion sound speed, on the measured ion velocities. However, the initial measurements shown in Figure 14B do not appear to scale as $n_e \propto (T_e)^{1/2}$ as would be expected if the flow velocity were dependent on the sound speed alone. However, more measurements are needed to make the trend more clear.

6. Conclusion

The MARIA helicon plasma source has been established as a reliable CW plasma source for basic plasma physics and plasma material interaction studies. Continuous operation of up to 1 kW of RF heating power has been demonstrated with magnetic field strengths up to 938 G and 2.0 mTorr neutral pressure. Under these conditions, electron densities of up to 6×10^{18} m^{-3} and temperatures in the range of 2-3 eV have been reached. Upgrading to a water cooled antenna, soon to be completed, is expected to enable CW operation at RF power up to 10 kW.

The focus on spectroscopic diagnostics has already yielded several insights in the behavior of helicon plasmas. LIF measurements have indicated a significant flow of ions along the axis of the device which is dependent on the neutral fill pressure. Expanding this line of inquiry can yield measurements

of the ion and neutral flux gradients and possibly a measurement of the ionization source distribution.

Acknowledgments

This work was funded by the National Science Foundation under NSF CAREER award PHY-1455210 and by funds of the Engineering Physics Department in the College of Engineering at the University of WisconsinMadison. The support and invaluable input and consultation of Prof Noah Hershkowitz on helicon plasmas is greatly appreciated.

References

[1] Caldwell A, Lotov K, Pukhov A and Simon F 2009 *Nature Physics* **5** 363–367
[2] Muggli P, Adli E, Apsimon R, Asmus F, Baartman R, Bachmann A M, Marin M B, Batsch F, Bauche J, Olsen V K B, Bernardini M, Biskup B, Vinuela E B, Boccardi A, Bogey T, Bohl T, Bracco C, Braunmuller F, Burger S, Burt G, Bustamante S, Buttenschön B, Butterworth A, Caldwell A, Cascella M, Chevallay E, Chung M, Damerau H, Deacon L, Dexter A, Dirksen P, Doebert S, Farmer J, Fedosseev V, Feniet T, Fior G, Fiorito R, Fonseca R, Friebel F, Gander P, Gessner S, Gorgisyan I, Gorn A A, Grulke O, Gschwendtner E, Guerrero A, Hansen J, Hessler C, Hofle W, Holloway J, Hüther M, Ibison M, Islam M R, Jensen L, Jolly S, Kasim M, Keeble F, Kim S Y, Kraus F, Lasheen A, Lefevre T, LeGodec G, Li Y, Liu S, Lopes N, Lotov K V, Martyanov M, Mazzoni S, Godoy D M, Mete O, Minakov V A, Mompo R, Moody J, Moreira M T, Mitchell J, Mutin C, Norreys P, Öz E, Ozturk E, Pauw W, Pardons A, Pasquino C, Pepitone K, Petrenko A, Pitmann S, Plyushchev G, Pukhov A, Rieger K, Ruhl H, Schmidt J, Shalimova I A, Shaposhnikova E, Sherwood P, Silva L, Sosedkin A P, Speroni R, Spitsyn R I, Szczurek K, Thomas J, Tuev P V, Turner M, Verzilov V, Vieira J, Vincke H, Welsch C P, Williamson B, Wing M, Xia G and Zhang H 2017 *Plasma Physics and Controlled Fusion* **60** 014046
[3] Buttenschön B, Fahrenkamp N and Grulke O 2018 *Plasma Physics and Controlled Fusion* **60** 075005
[4] Sudit I D and Chen F F 1999 *Plasma Sources Science and Technology* **5** 43 – 53
[5] Blackwell B D, Caneses J F, Samuell C M, Wach J, Howard J and Corr C 2012 *Plasma Sources Science and Technology* **21** 055033
[6] Miljak D G and Chen F F 1999 *Plasma Sources Science and Technology* **7** 537–549
[7] Denning C M 2008 *Neutral Depletion and Ion Acceleration in an Argon Helicon Plasma* Ph.D. thesis University of Wisconsin - Madison
[8] Liard L, Aanesland A and Chabert P 2012 *Journal of Physics D: Applied Physics* **45** 235201
[9] Keesee a M and Scime E E 2007 *Plasma Sources Science and Technology* **16** 742–749
[10] Magee R M, Galante M E, Carr J, Lusk G, McCarren D W and Scime E E 2013 *Physics of Plasmas* **20** 2–6
[11] Galante M E, Magee R M and Scime E E 2014 *Physics of Plasmas* **21** 055704
[12] Chen F F 2015 *Plasma Sources Science and Technology* **24** 014001
[13] Schmitz O, Beigman I L, Vainshtein L A, Schweer B, Kantor M, Pospieszczyk A, Xu Y, Krychowiak M, Lehnen M, Samm U and Unterberg B 2008 *Plasma Physics and Controlled Fusion* **50** 115004 ISSN 0741-3335
[14] Chen F F 1996 *Physics of Plasmas* **3** 1783–2797
[15] Davies B 1970 *Journal of Plasma Physics* **4** 43
[16] Boswell R W 1984 *Journal of Plasma Physics* **31** 197
[17] Davies B and Christiansen P J 1969 *Plasma Physics* **11** 987–1000
[18] Ferrari R L and Klozenberg J P 1968 *Journal of Plasma Physics* **2** 283
[19] Klozenberg J P, McNamara B and Thonemann P C 1965 *Journal of Fluid Mechanics* **21** 545 ISSN 0022-1120
[20] Chen F F and Arnush D 1997 *Physics of Plasmas* **4** 3411–3421
[21] Blackwell D D, Madziwa T G, Arnush D and Chen F F 2002 *Physical Review Letters* **88** 145002
[22] Isayama S, Hada T, Shinohara S and Tanikawa T 2016 *Physics of Plasmas* **23** 0–6 ISSN 10897674
[23] Carter M D, Baity F W, Barber G C, Goulding R H, Mori Y, Sparks D O, White K F, Jaeger E F, Chang-Díaz F R and Squire J P 2002 *Physics of Plasmas* **9** 5097 – 5110
[24] Sudit I D and Chen F F 1994 *Plasma Sources Science and Technology* **3** 162–168
[25] Chen F F 2012 *Plasma Sources Science and Technology* **21** 055013
[26] Chen F F 2001 *Physics of Plasmas* **8** 3029–3041
[27] Hershkowitz N 1989 How Langmuir Probes Work *Plasma Diagnostics, Discharge Parameters and Chemistry* (Academic Press, Inc) ISBN 978-1-4832-0281-5
[28] Tango W J, Link J K and Zare R N 1968 *The Journal of Chemical Physics* **49** 4264–4268
[29] Severn G D, Edrich D A and McWilliams R 1998 *Review of Scientific Instruments* **69** 10
[30] Green J, Schmitz O, Severn G and Winters V 2019 *Measurement Science and Technology* **30** 055202